Monthly Notices
of the
ROYAL ASTRONOMICAL SOCIETY

MNRAS **462,** S235–S241 (2016)
Advance Access publication 2016 October 5

doi:10.1093/mnras/stw2480

Magnetic field pile-up and draping at intermediately active comets: results from comet 67P/Churyumov–Gerasimenko at 2.0 AU

C. Koenders,[1] C. Goetz,[1]★ I. Richter,[1] U. Motschmann[2,3] and K.-H. Glassmeier[1,4]

[1]*Institut für Geophysik und extraterrestrische Physik, Technische Universität Braunschweig, Mendelssohnstraße 3, D-38106 Braunschweig, Germany*
[2]*Institut für theoretische Physik, Technische Universität Braunschweig, Mendelssohnstraße 3, D-38106 Braunschweig, Germany*
[3]*DLR-Institut für Planetenforschung, Rutherfordstr. 2, D-12489 Berlin, Germany*
[4]*Max-Planck Institut für Sonnensystemforschung, Justus-von-Liebig-Weg 3, D-37077 Göttingen, Germany*

Accepted 2016 October 4. Received 2016 September 27; in original form 2016 June 13

ABSTRACT

The interaction between a comet and the impinging solar wind leads to modifications of the magnetic field in the environment of a comet. Among those, one finds magnetic field pile-up and draping, which reveal properties of the interaction and are known from previous cometary spacecraft missions. This work studies the magnetic field configuration at comet 67P/Churyumov–Gerasimenko at 2.0 AU. The data reveal a pile-up of the magnetic field and a draping signature nearly perpendicular to the original solar wind flow and the plane containing the solar wind flow and the interplanetary magnetic field. A comparison of the magnetic field data with a hybrid plasma simulation supports this idea of a plasma flow which is strongly deflected from the Sun–comet direction and which is in line with other plasma observations by the Rosetta Plasma Consortium.

Key words: magnetic fields – plasmas – methods: data analysis – methods: numerical – comets: individual: 67P/Churyumov–Gerasimenko.

1 INTRODUCTION

Solar insolation leads to the sublimation of the cometary ices. This neutral gas escapes from the nucleus and forms an extended cometary neutral atmosphere, which acts as an obstacle for the impinging solar wind ions and electrons. By means of photoionization and charge-exchange, these neutral molecules are ionized and the interaction between the comet and the solar wind is enhanced. Within this interaction region, the solar wind flow is modified and various structures and boundaries form. The actual strength of the interaction depends on the gas production rate of the comet and properties of the impinging solar wind.

The impinging solar wind is accompanied by the interplanetary magnetic field. Due to the electrically conducting nature of the solar wind, a modification of the solar wind flow also leads to changes in the magnetic field. This was initially proposed by Alfvén (1957), who discussed the formation of cometary tails and the associated magnetic field draping. In this model, the interplanetary magnetic field is frozen in the solar wind flow. The solar wind is slowed down by the incorporation of heavy cometary ions into the solar wind flow, the so-called mass-loading, in the close vicinity of the comet. It is still moving with undisturbed speed far away from the nucleus. Consequently, the magnetic field, which is frozen in the flow, is wrapped around the comet (Israelevich & Ershkovich 1994; Israelevich, Neubauer & Ershkovich 1994). In a simple way, this leads to a draped magnetic field at the comet and, in extension, the formation of a comet's tail.

Besides this draping effect, the magnetic field also piles up ahead of the comet because the solar wind flow is decelerated. In case of a complete stagnation of the solar wind flow upstream of the comet, the magnetic field strength is proportional to the dynamic pressure of the solar wind (cf. Huddleston, Coates & Johnstone 1992).

Observations made with spacecraft indeed show the draping and the pile-up of the magnetic field. For example, Smith et al. (1986) reported that the *ICE* spacecraft crossed a two-lobed comet tail 7800 km downstream of the cometary nucleus. In these lobes, the magnetic field is oppositely directed and the magnetic field component along the Sun–comet axis is dominating the field, i.e. in one lobe the magnetic field is oriented towards the Sun, whereas in the other lobe it is orientated away from the Sun. Furthermore, the authors reported on field strengths of about 60 nT. Similar field strengths have been observed by the magnetometer on board the *Giotto* spacecraft, passing comet 1P/Halley (Neubauer et al. 1986). Raeder et al. (1987) analysed the draping configuration from that mission and found several draping signatures, which are caused by previous changes of the interplanetary magnetic field orientation. This has been revisited by Volwerk et al. (2014), who also analysed the draping configuration observed during the *VEGA 1* and *VEGA 2* flybys, which reveal a similar draping mostly in sunward- and antisunward-direction. Similar observations have been reported by various other authors (cf. Richter et al. 2011; Delva et al. 2014).

★ E-mail: c.goetz@tu-bs.de

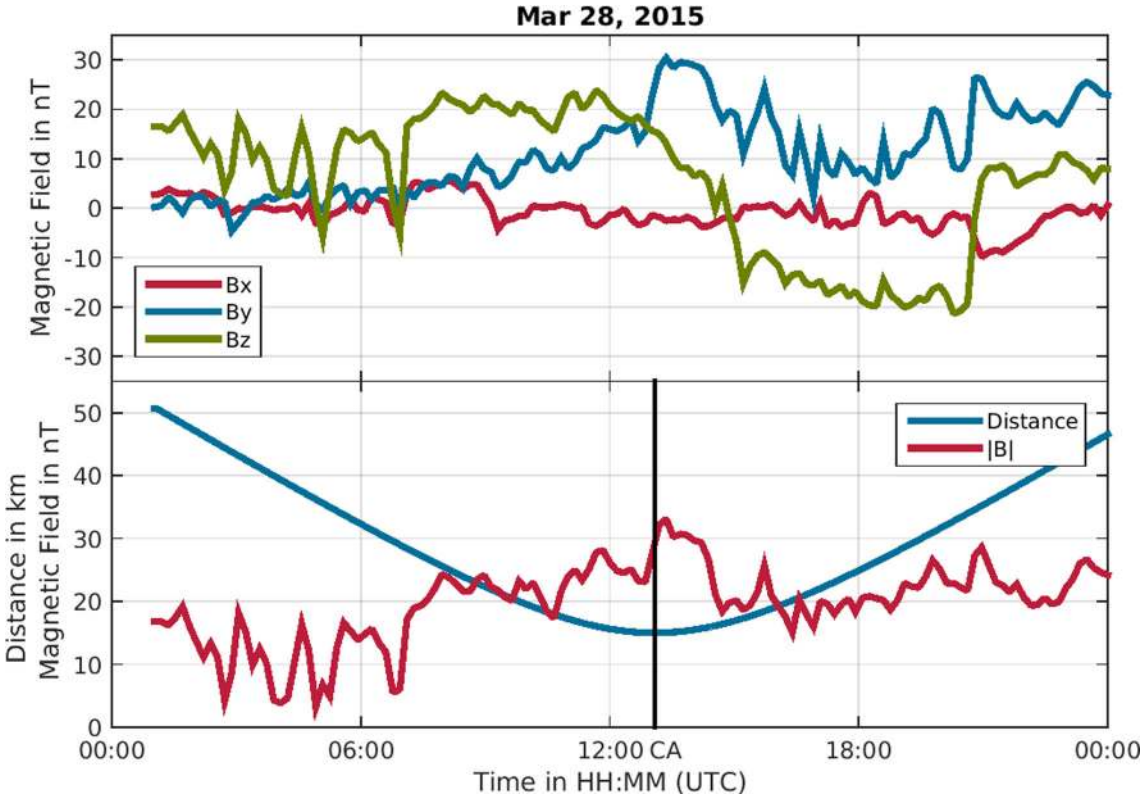

Figure 1. Magnetic field data on the 2015 March 28th (60 s average). The top panel shows the components of the magnetic field in CSEQ, in which the red line shows B_x, the blue line B_y, and the green line B_z, respectively. The bottom panel shows the magnitude of the magnetic field and the distance to the comet. The spacecraft passed the point of closest approach at 13:05 UTC (vertical black line) at a distance of 15 km.

Numerical simulations of the interaction between the solar wind and a strongly active comet show that a bilobed magnetic field configuration is present and that in this draping signature the magnetic field component along the Sun–comet line is dominating (cf. Gombosi et al. 1996). Recent simulations of the interaction of 67P/Churyumov–Gerasimenko close to its perihelion indicate that the magnetic field component parallel to the Sun–comet line is dominant. In contrast to the simulations at comet 1P/Halley, an asymmetry in the plasma structures is present at 67P/Churyumov–Gerasimenko, which distinguishes two hemispheres, one with high solar wind ion density and one with high cometary ion density. It is caused by the acceleration of cometary ions and a resulting deflection of the solar wind in the opposite direction (cf. Koenders et al. 2015; Rubin et al. 2015). The gas production rate of the comet decreases with the increasing asymmetry. However, at weakly active comets, meaning at very low gas production rates, the deflection of the flow is very small again. Thus, the simulations suggest that the asymmetry peaks at an intermediate activity stage. In addition, weakly active comets reveal only a slightly enhanced magnetic field and, consequently, a much weaker pile-up and draping of the magnetic field, as simulations suggest (Rubin et al. 2014; Koenders et al. 2016).

The measurements shown here were made with the instruments of the Rosetta Plasma Consortium (RPC; Carr et al. 2007) on board the *Rosetta* spacecraft (Glassmeier et al. 2007a). A highlight of the *Rosetta* mission is observations of the evolution of the plasma environment from the weakly to the strongly active phases because it escorts the comet during its journey around the Sun. In agreement with these simulations, Richter et al. (2015, 2016) reported on mean magnetic field strengths in the low-activity phase of the comet below 10 nT at 20–30 km distance to the nucleus, which is just a few times the undisturbed interplanetary magnetic field strength. This indicates that there is only a weak pile-up. In addition, Broiles et al. (2015) and Behar et al. (2016a,b) show that the solar wind flow is only weakly deflected in the first months after spacecraft arrival at the comet in 2014 August, but the deflection increases with the increasing gas production rate of the comet, at least until mid-2015 March at a heliocentric distance of 2 AU. This is still five months ahead of the comet's perihelion passage at 1.24 AU in 2016 August.

The aim of this paper is a description of the magnetic field measurements (Glassmeier et al. 2007b) at a heliocentric distance of 2 AU. Based on simulation studies, the corresponding activity stage is the intermediate stage between the weakly active comet and the strongly active comet, where structures and boundaries are present (e.g. Goetz et al. 2016a,b). Therefore, we study the magnetic field draping and pile-up during the second close-flyby of *Rosetta* on 2015 March 28th. We also compare the magnetic field measurements with a hybrid plasma simulation, which finally allows us to reconstruct a global state of the plasma environment at the comet at this point in time.

2 OBSERVATIONS

For most of its first months at the comet, the *Rosetta* spacecraft stayed in bound orbits close to the terminator plane of the nucleus. During these orbits, the radial coverage of the measurements was negligibly small or performed over time-scales where the orientation in the interplanetary magnetic field and, therefore, the orientation of the entire plasma environment changed several times (cf. Rubin et al. 2014; Broiles et al. 2015; Behar et al. 2016b). But the spacecraft also

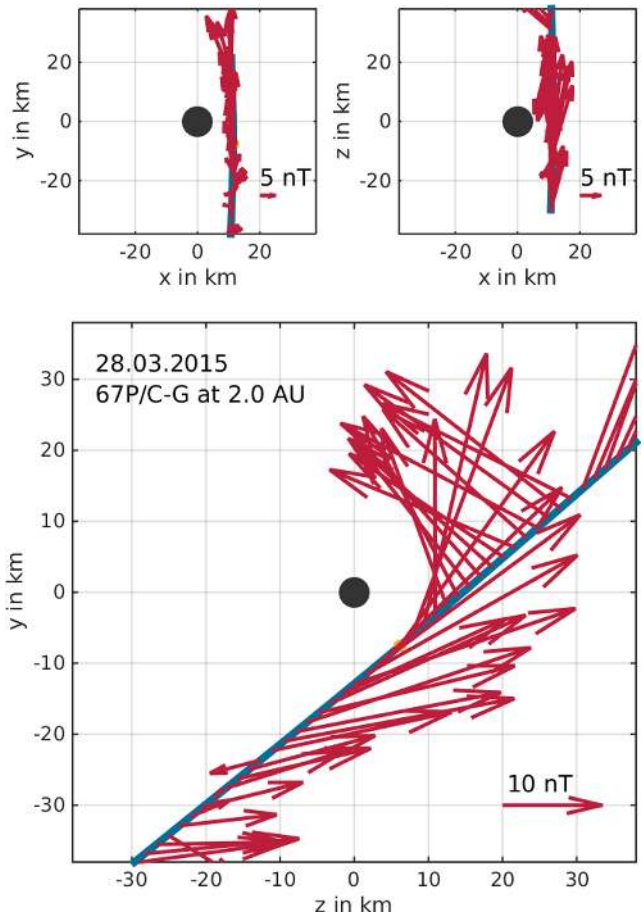

Figure 2. The orbit and the orientation of the magnetic field. The top-left panels shows the *xy*-plane, and the *xz*-plane is shown in the top-right panel. The bottom panel shows the orbit and the magnetic field orientation in the *yz*-panel. All coordinates and magnetic fields are given in the CSEQ system, the Sun is in the positive *x*-direction.

performed two so-called close flybys. This means *Rosetta* started at an intermediate distance and then passed the nucleus at a much smaller distance before it moved away from the nucleus. This orbit type is preferred for a study of the magnetic field draping due to its large radial changes.

One of these close flybys took place on 2015 March 28th, when *Rosetta* started at about 50 km to the nucleus and dipped down to a minimum distance of 15 km at about 13:05 UTC. At 01:00 on that day the RPC-MAG (Glassmeier et al. 2007b) instrument was switched into burst mode, which measures the magnetic field with a sampling frequency of 20 vectors s^{-1}. The magnetic field data is cleaned by a temperature model obtained from cavity crossings by Goetz et al. (2016a, this issue). The authors report that the resulting spacecraft bias fields are below 5 nT. Since we are interested in the large-scale behaviour of the magnetic field, we use data averaged over 60 s (Fig. 1). Around 00:00 UTC the next day, the spacecraft reached again a distance of about 50 km (Fig. 1). In the comet-centred solar equatorial frame (CSEQ), the flyby orbit is about constant in *x*-direction and upstream of the nucleus. The spacecraft moves from $(-y, -z)$ to $(+y, +z)$ (Fig. 2); this trajectory is approximately perpendicular to the comet–sun line and out of the ecliptic. In the CSEQ frame used here, the *x*-axis points towards the Sun, the *z*-axis is parallel to the component of the solar north pole that is orthogonal to the *x*-axis, and the *y*-axis completes the right-handed coordinate system. The nucleus is at the origin.

The mean magnetic field strength on that day was about 20 nT, which is about seven times the nominal strength (2.8 nT) of the undisturbed interplanetary magnetic field at that heliocentric distance (Hansen et al. 2007). This indicates that the strength of the comet–solar wind interaction increased compared to the first months at the comet (Richter et al. 2015). The magnetic field strength during this flyby increased towards the point of closest approach. Between 01:00 and 12:00, it was about 15 nT, but with several deep dips. Towards closest approach, it increased; the averaged data shows a maximum value of 33 nT. Afterwards, the magnetic field strength decreased again to values of about 20 to 25 nT.

The inspection of the components reveals that the field strength at closest approach is governed by the B_y component, which peaks at this point. At 01:00 UT, it was close to 0 nT and around 10 nT at 18:00 UT. At these times, the field strength was mainly determined by the *z*-component. This component changed its sign from 07:00 UT towards 18:00 UT. At 20:45 UT, a rotation took place, where B_z again changed the sign. But it is remarkable that the B_x component was close to zero the entire day.

Fig. 2 displays the orientation of the magnetic field along the orbit. A clear flip in the orientation is visible close to the point of closest approach. Thus, on the $-y$-hemisphere the magnetic field points towards $+z$-direction, whereas it points in nearly the opposite direction on the $+y$-hemisphere. This is a characteristic signature of field draping. However, in contrast to all previous observations of draping at comets, the dominant draping signature is not in the *x*-direction, which remains between -9 and 5 nT in the 60 s-data on that day. Instead, it is the *z*-direction. This indicates that the plasma flow, which transports the magnetic field and by this leads to the clear draping signature, is not coming from the Sun direction. It rather moves from $+z$ direction and towards the $-z$-hemisphere. This is true at least in the innermost coma, where measurements are available.

3 SIMULATION SETUP

In order to obtain information on the state of the global plasma interaction, we use a plasma simulation. As shown by Rubin et al. (2014), Koenders et al. (2015), and Koenders et al. (2016), hybrid plasma simulations are appropriate means to describe the cometary plasma environment of weakly as well as strongly active comets. In this model, the ions are described as particles, whereas the electrons are described as a fluid. Hence, the model is able to describe the kinetic effects of the solar wind protons as well as those of the cometary ions. Details of the simulation tool, the A.I.K.E.F. code, are given in Müller et al. (2011).

In this study, we consider photoionization, charge-exchange, ion-neutral collisions, recombination and electron–water excitation as processes in the cometary environment. See Koenders et al. (2013, 2015, 2016) for details. As a consequence of the bilobed shape of the nucleus, the neutral gas distribution in the coma is anisotropic (Bieler et al. 2015; Hässig et al. 2015); thus, we refrain from using the radially symmetric model by Haser (1957), instead the simulation uses the empirical model by Hansen (2016, this issue), which is a fit to the neutral gas coma of Bieler et al. (2015) averaged over an entire comet rotation. Consequently, we do not aim for a time-dependent comparison of the flyby, which lasts more than two comet rotations. Rather the simulation shows the general behaviour of the plasma interaction. The empirical neutral gas model leads to an enhanced neutral gas density on the day side and, in

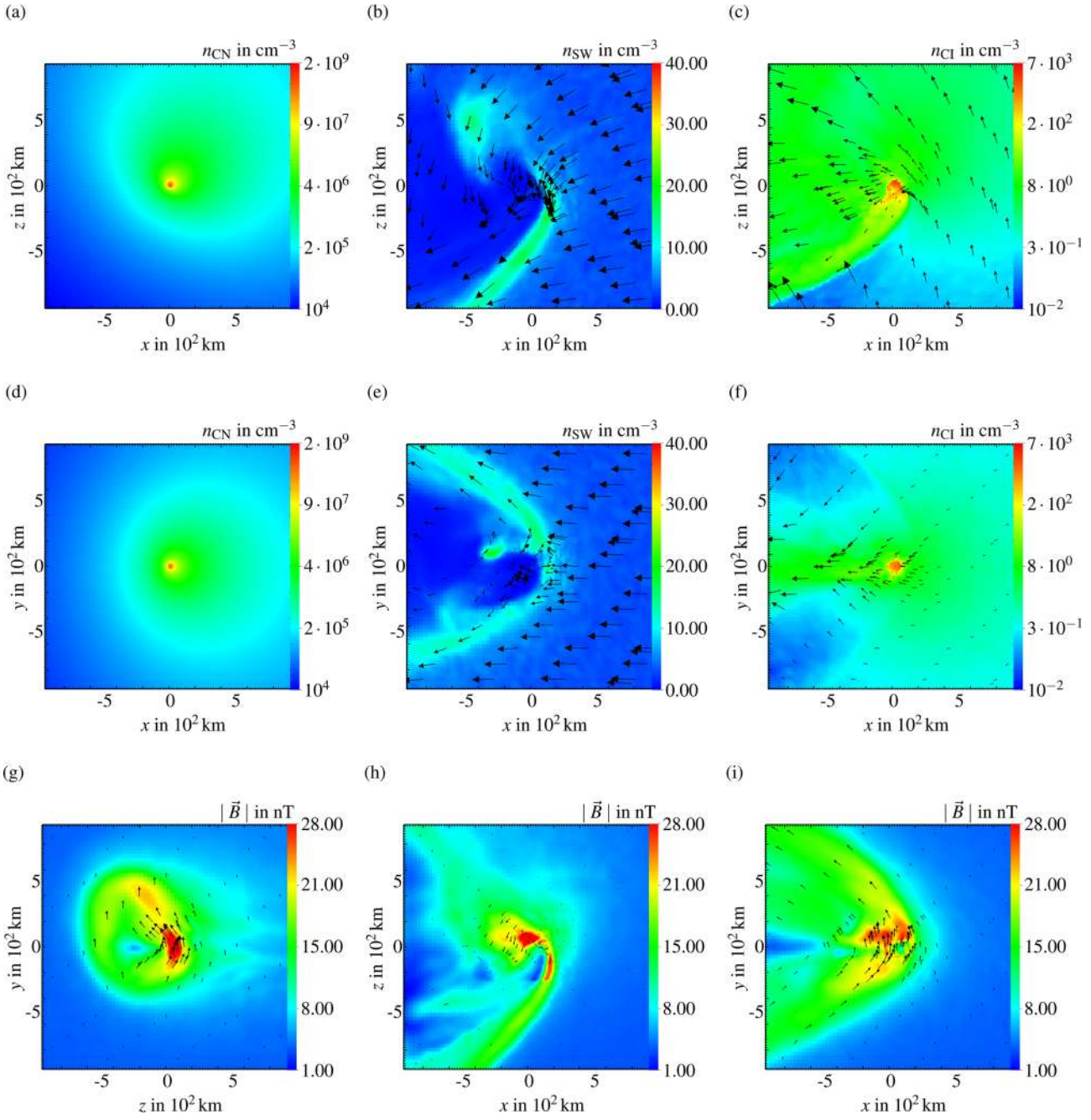

Figure 3. The hybrid simulations results. Panels (a) and (d), (b) and (e), and (c) and (f) show the cometary neutral density, the solar wind proton density and its bulk velocity, and the cometary ion density and its bulk velocity on the $y = 0$- and the $z = 0$-cross-section, respectively. The magnetic field strength and its direction is shown in the panels (g) to (i). The solar wind approaches the comet from the $+x$ direction, corresponding to the CSEQ system. The interplanetary magnetic field is in the $(+x, +y)$ plane with a Parker angle of 63°. For more details, see the text.

addition, the maximum density is shifted towards northern latitudes. Hansen (2016, this issue) also gives a good estimation on the total gas production rate of the comet, which is based on a fit of three day averaged measurements by various *Rosetta* instruments. The conditions in the undisturbed solar wind ahead of the comet during that flyby are unknown as well, so we use standard solar wind conditions at 2.0 AU (Hansen et al. 2007). To incorporate the anisotropic neutral gas density in the simulation, it is necessary to relate the comet's frame of reference to the CSEQ frame; however, the orientation of the interplanetary magnetic field with respect to the nucleus is not known, so that we assume that the comet's rotation axis is parallel to the z-direction for this simulation (Fig. 3 a and d). The physical parameters of the simulation are listed in Table 1. The significant plane in the solar wind is the xy-plane which contains the solar wind bulk velocity and the interplanetary magnetic field.

The simulation box is a cube with 8600 km along each axis. The undisturbed solar wind moves in $-x$-direction in the CSEQ frame, which is used in this simulation as well. The interplanetary magnetic field is only in the xy-plane with $B_x = 1.3$ nT and $B_y = 2.5$ nT, resulting in a field magnitude of 2.8 nT. The solar wind convective electric field points towards $+z$-direction. The numerical mesh in the simulation is hierarchically structured with three levels.

Table 1. Solar wind conditions at 2.0 AU (Hansen et al. 2007) and neutral gas parameters by Hansen (2016, this issue).

Quantity		Value
Interplanetary magnetic field	B_{IMF}	2.8 nT
Parker angle	θ	63°
Solar wind density	n_{SW}	2.5 cm^{-3}
Solar wind speed	u_{SW}	400 km s^{-1}
Photoionization rate	ν	2.5×10^{-7} s^{-1}
Gas production rate	Q	7×10^{26} s^{-1}
Neutral gas speed	u_{NG}	660 m s^{-1}

Its coarsest resolution is 60 km and the finest, which is closest to the origin, about 7 km. The nucleus is not modelled in the simulation. In order to stabilize the simulation, the magnetic and electric fields are smoothed.

4 SIMULATION RESULTS AND DISCUSSION

The results of the hybrid simulation are presented in Fig. 3. Similar to the observations in Koenders et al. (2016), it shows that the cometary ion density reveals two regions: an inner region with an enhanced cometary ion density and an outer region with a lower density where the cometary ions are accelerated by the convective electric field of the solar wind (panel c). This points into $+z$-direction in the undisturbed solar wind. However, due to the pick-up of the cometary ions, the solar wind is deflected and with it the direction of the convective electric field. This also affects the cometary ion motion. In contrast to this outer region, the cometary ions in the inner region move towards $(-x, 0, -z)$-direction, and thus perpendicular to the solar wind plane, with a much slower speed. The inner region extends up to 100 km in Sun direction, which is caused by the stronger gas production rate and the anisotropic neutral gas distribution. The transition between these two regions is rather sharp, which is an indication for the presence of two plasma regions. A similar transition has been observed by Yang et al. (2016, this issue) using measurements of RPC-LAP (Eriksson et al. 2006) during the approach phase in autumn 2014.

As mentioned above, the solar wind is deflected due to the presence of the cometary ions. This has been reported by various simulations and observational studies (cf. Rubin et al. 2014; Broiles et al. 2015; Behar et al. 2016a,b; Koenders et al. 2016). Behar et al. (2016a) found a peak value in the deflection out of the xy-plane of about 90° in early 2015 March. However, this single value might be caused by a short-time magnetic field enhancement. But nevertheless, in late February the mean deflection was about 50°. In the current simulation, which covers a time period at the end of March, the deflection away from the undisturbed solar wind direction reaches values of about 90° in the Mach cone and even larger values in the region behind the Mach cone close to the comet. However, the solar wind density is strongly depleted in this region, which indicates the formation of an ion composition boundary (cf. Koenders et al. 2015).

In contrast to the interaction at weakly active comets (Rubin et al. 2014; Koenders et al. 2016) the opening angle of the Mach cone near the nucleus is much larger, which seems to be similar to a cometary bow shock. However, in contrast to a fully established cometary bow shock, this Mach cone is only present on the $-z$-hemisphere. In the $+z$-hemisphere, strong fluctuations occur, which indicate the beginning of the formation of boundaries.

The magnetic field configuration close to the nucleus is shown in Fig. 4. The simulation shows that the B_y component is the dominant one close the nucleus. It is enhanced by a factor of 10 compared to the initial solar wind value, reaching about 30 nT, which is close to the value observed during the flyby. However, the position of this maximum differs from the observation, which is probably caused by the coarse resolution of the numerical mesh. The maximum magnetic field strength, which can be generated by transforming the dynamic ram pressure of the solar wind into magnetic pressure, would be $B_{max} = 40$ nT (cf. Huddleston et al. 1992). This value is above the peak values in the simulation and at the comet, which indicates that the plasma flow is not completely stopped or that parts of the pressure are transformed to thermal pressure.

Similar to the observation, the simulation reveals a draping in z-direction. However, in contrast to the observation, the z-component is about a factor of 2 smaller. In addition, when comparing Figs 2 and 4, it becomes apparent that the distance between the two regions of opposite polarity of B_z is larger than in the measurements, which could be caused by the limited spatial resolution or by the use of the averaged neutral gas density profile. Furthermore, the simulation and the observation reveal that the strength of B_z is similar in both lobes, which indicates that the assumption of a zero B_z-component in the undisturbed interplanetary magnetic field is correct. In general, the simulation shows a similar draping signature as the measurements.

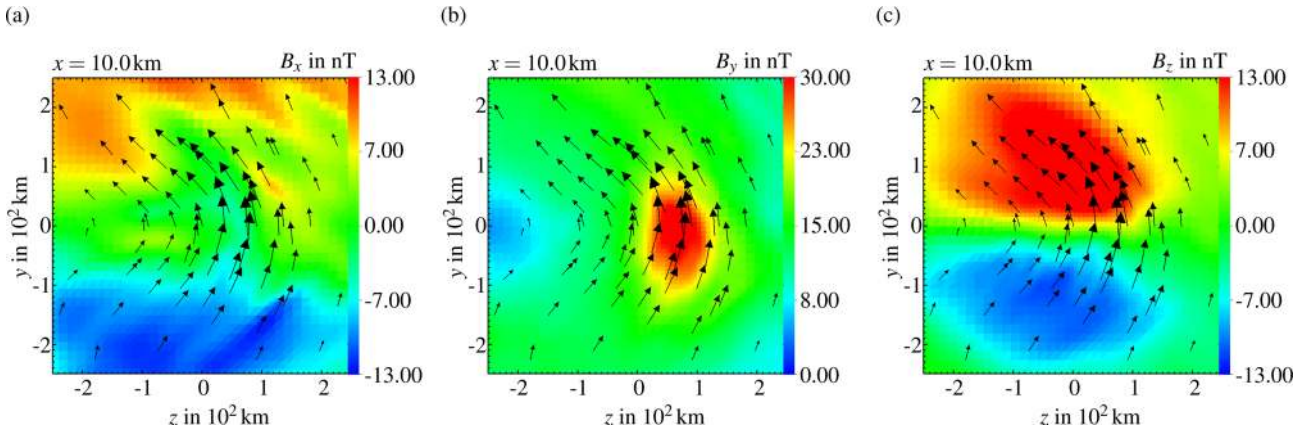

Figure 4. The simulated magnetic field in the cross-section $x = 10$ km upstream of the comet. In (a), (b), and (c), the B_x, B_y, and B_z components of the magnetic field are shown, respectively. In addition, each panel shows the projection of the magnetic field vectors on that cross-section.

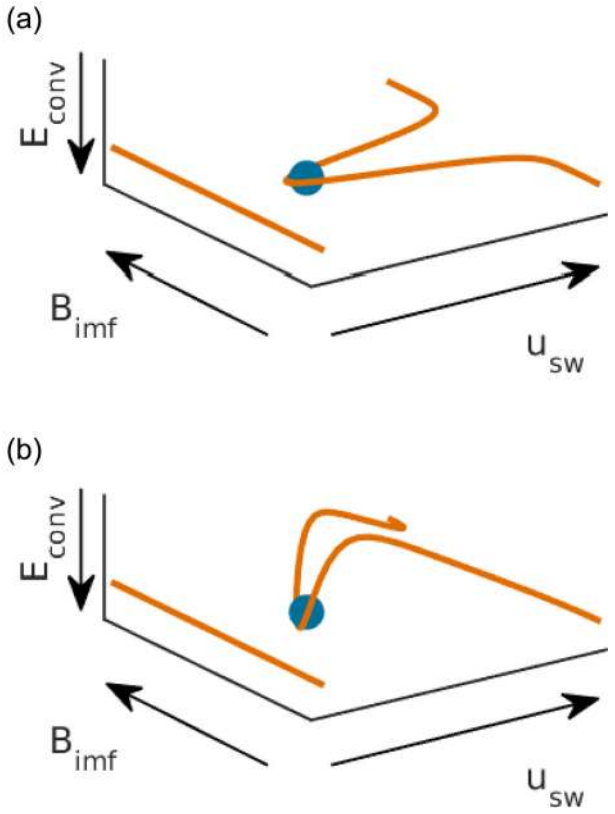

Figure 5. A sketch of the magnetic field configurations at comets. The field line configuration at a strongly active comet (cf. Alfvén 1957) is shown in panel (a), which is confined to the *xy*-plane, i.e. the plane containing the solar wind flow and magnetic field. In contrast, the draping signature at intermediately active comets is shown in panel (b). Due to the strong deflection of the plasma flow in the interaction region, the entire field line is moved in $-\vec{E}_{\rm conv}$-direction. However, the field line is also draped around the denser region close to the nucleus, which leads to a plasma tail that is perpendicular to the Sun–comet line close to the nucleus.

Thus, we can conclude from the *Rosetta* magnetic field measurements that the magnetic field draping perpendicular to the undisturbed solar wind flow is probably not caused by a special solar wind configuration, rather it is a general feature present at comets at an intermediate-activity stage. A sketch of the draping configuration is presented in Fig. 5. As a consequence of the draping signature, we can confirm that the cometary plasma tail, i.e. the location where the density of cometary ions is highest, is perpendicular to the comet–Sun direction, at least in the inner interaction region.

In addition, neither the observation nor the simulation reveal a presence of a diamagnetic cavity at a distance of about 10 km to the nucleus. In the simulation, this could be caused by the limited spatial resolution of about 7 km, while the measurements gives at least an upper limit of about 10 km to the surface. This value is a factor of 5 or 12 smaller than the corresponding values calculated with the fits of the diamagnetic cavity size determined by Goetz et al. (2016a, this issue) during the more active period in summer and autumn 2015. Thus, this might either indicate that the cavity has not formed yet, or, more likely, that the stability of the cavity differs from that in the more active period.

5 CONCLUSION

This work studies the magnetic field observation during the close flyby on 2015 March 28th of the *Rosetta* spacecraft at comet 67P/Churyumov–Gerasimenko at 2.0 AU, before it reached its perihelion. The magnetic field reaches a maximum field strength of about 33 nT, which is close to the maximum value theoretically predicted, indicating that the plasma flow close to the comet is nearly stopped. However, the observations do not reveal the presence of a diamagnetic cavity along the flyby trajectory. Thus, if there was a cavity at the comet during that time, the cavity size must have been smaller than 10 km.

Furthermore, the data show a strong draping signature, which is in the *z*-component of the magnetic field being perpendicular to the plane containing the magnetic field and particle flow in the undisturbed solar wind. This is in contrast to all other draping observations at comets which have previously been visited by spacecraft. It is a strong indication that the plasma flow at this intermediate-activity stage is strongly deflected from the Sun–comet direction.

Besides the magnetic field measurements by RPC-MAG, we presented a hybrid simulation of this interaction. The simulation supports the observation of a strongly deflected plasma flow, which finally leads to the draping signature in the *z*-component. These points are also in agreement with previous studies (cf. Broiles et al. 2015; Behar et al. 2016a,b). This study proves that at 2.0 AU the plasma tail of comet 67P/Churyumov–Gerasimenko is, close to the nucleus, perpendicular to the Sun–comet line.

ACKNOWLEDGEMENTS

The hybrid simulations were performed on the system of the North-German Supercomputing Alliance. *Rosetta* is a European Space Agency (ESA) mission with contributions from its member states and the National Aeronautics and Space Administration (NASA). The work on RPC-MAG was financially supported by the German Ministerium für Wirtschaft und Energie and the Deutsches Zentrum für Luft- und Raumfahrt under contract 50QP 1401. We are indebted to the whole of the *Rosetta* Mission Team, SGS, and RMOC for their outstanding efforts in making this mission possible. The RPC-MAG data presented here have been made available through the PSA archive of ESA and the PDS archive of NASA.

REFERENCES

Alfvén H., 1957, Tellus, 9, 92
Behar E., Lindkvist J., Nilsson H., Ramstad R., 2016a, A&A, in press
Behar E., Nilsson H., Wieser G. S., Nemeth Z., Broiles T. W., Richter I., 2016b, Geophys. Res. Lett., 43, 1411
Bieler A. et al., 2015, A&A, 583, A7
Broiles T. et al., 2015, A&A, 583, A21
Carr C. et al., 2007, Space Sci. Rev., 128, 629
Delva M., Bertucci C., Schwingenschuh K., Volwerk M., Romanelli N., 2014, Planet. Space Sci., 96, 125
Eriksson A. I. et al., 2006, Space Sci. Rev., 128, 729
Glassmeier K.-H., Boehnhardt H., Koschny D., Kührt E., Richter I., 2007a, Space Sci. Rev., 128, 1
Glassmeier K.-H. et al., 2007b, Space Sci. Rev., 128, 649
Goetz C. et al., 2016a, MNRAS, in press
Goetz C. et al., 2016b, A&A, 588, A24
Gombosi T. I., De Zeeuw D. L., Häberli R. M., Powell K. G., 1996, J. Geophys. Res., 101, 15233
Hansen K. C., 2016, MNRAS, in press
Hansen K. C. et al., 2007, Space Sci. Rev., 128, 133
Haser L., 1957, Bull. Soc. R. Sci. Liege, 43, 740

Hässig M. et al., 2015, Science, 347, aaa0276
Huddleston D. E., Coates A. J., Johnstone A. D., 1992, Geophys. Res. Lett., 19, 837
Israelevich P. L., Ershkovich A. I., 1994, J. Geophys. Res., 99, 21225
Israelevich P. L., Neubauer F. M., Ershkovich A. I., 1994, J. Geophys. Res., 99, 6575
Koenders C., Glassmeier K.-H., Richter I., Motschmann U., Rubin M., 2013, Planet. Space Sci., 87, 85
Koenders C., Glassmeier K.-H., Richter I., Ranocha H., Motschmann U., 2015, Planet. Space Sci., 105, 101
Koenders C., Perschke C., Goetz C., Richter I., Motschmann U., Glassmeier K. H., 2016, A&A, 594, A66
Müller J., Simon S., Motschmann U., Schüle J., Glassmeier K.-H., Pringle G. J., 2011, Comput. Phys. Commun., 182, 946
Neubauer F. M. et al., 1986, Nature, 321, 352
Raeder J., Neubauer F. M., Ness N. F., Burlaga L. F., Raeder J., Neubauer F. M., Ness N. F., Burlaga L. F., 1987, A&A, 187, 61
Richter I., Koenders C., Glassmeier K.-H., Tsurutani B. T., Goldstein R., 2011, Planet. Space Sci., 59, 691
Richter I. et al., 2015, Ann. Geophys., 33, 1031
Richter I. et al., 2016, Ann. Geophys., 34, 609
Rubin M. et al., 2014, Icarus, 242, 38
Rubin M., Gombosi T. I., Hansen K. C., Ip W., Kartalev M. D., Koenders C., Toth G., 2015, Earth Moon Planets, 116, 141
Smith E. J., Tsurutani B. T., Salvin J. A., Jones D. E., Siscoe G. L., Mendis D. A., 1986, Science, 232, 382
Volwerk M., Glassmeier K.-H., Delva M., Schmid D., Koenders C., Richter I., Szegö K., 2014, Ann. Geophys., 32, 1441
Yang L., Paulsson J., Wedlund C. S., Odelstad E., Edberg N. J. T., Miloch W. J., Eriksson A. I., 2016, A&A, in press

This paper has been typeset from a TEX/LATEX file prepared by the author.